

AC-LIO: Towards Asymptotic Compensation for Distortion in LiDAR-Inertial Odometry via Selective Intra-Frame Smoothing

Tianxiang Zhang, Xuanxuan Zhang, Wenlei Fan, Xin Xia, Huai Yu, Lin Wang, and You Li

Abstract—Existing LiDAR-Inertial Odometry (LIO) methods typically utilize the prior trajectory derived from the IMU integration to compensate for the motion distortion within LiDAR frames. However, discrepancies between the prior and true trajectory can lead to residual motion distortions that compromise the consistency of LiDAR frame with its corresponding geometric environment. This imbalance may result in pointcloud registration becoming trapped in local optima, thereby exacerbating drift during long-term and large-scale localization. To this end, we propose a novel LIO framework with selective intra-frame smoothing dubbed AC-LIO. Our core idea is to asymptotically backpropagate current update term and compensate for residual motion distortion under the guidance of convergence criteria, aiming to improve the accuracy of discrete-state LIO system with minimal computational increase. Extensive experiments demonstrate that our AC-LIO framework further enhances odometry accuracy compared to prior arts, with about 30.4% reduction in average RMSE over the second best result, leading to marked improvements in the accuracy of long-term and large-scale localization and mapping. Our code and demo are available on <https://cyberkona.github.io/publication/ac-lio/>.

Index Terms—LiDAR-inertial odometry (LIO), simultaneous localization and mapping (SLAM), asymptotic distortion compensation, convergence criteria, selective intra-frame smoothing.

I. INTRODUCTION

WITH the advancements in Simultaneous Localization and Mapping (SLAM) technology, robots are increasingly achieving precise perception of external environments and their own motion [1]–[3]. As a vital subset of SLAM, LiDAR-Inertial Odometry (LIO) has gained widespread application in autonomous driving [4], unmanned logistics [5] and other fields, for its high robustness and accuracy [6], [7]. Compared to Visual-Inertial Odometry, LIO system can directly obtain depth observations of surroundings, without the need to estimate the depth of feature points [8], and exhibits better adaptability to different lighting conditions [9], [10].

However, as LIO system continues to evolve, there still remain several fundamental issues to be addressed [11]–[13]. One of them is the conflict between continuous motion and rigid pointcloud registration [14]. Since the acquisition of

¹T. Zhang, X. Zhang, W. Fan, and Y. Li are with State Key Laboratory of Information Engineering in Surveying, Mapping and Remote Sensing (LIESMARS), Wuhan University, China. X. Zhang is the corresponding author. Email: {cyberkona; xuanxuanzhang; wenleifan; liyou}@whu.edu.cn

²Xin Xia is with Department of Mechanical Engineering, University of Michigan-Dearborn. Email: xinxia@umich.edu

³H. Yu is with Electronic Information School, Wuhan University, China. Email: yuhuai@whu.edu.cn

⁴T. Zhang, L. Wang are with School of Electrical and Electronic Engineering, Nanyang Technological University, Singapore. Email: n2409916c@e.ntu.edu.sg; linwang@ntu.edu.sg

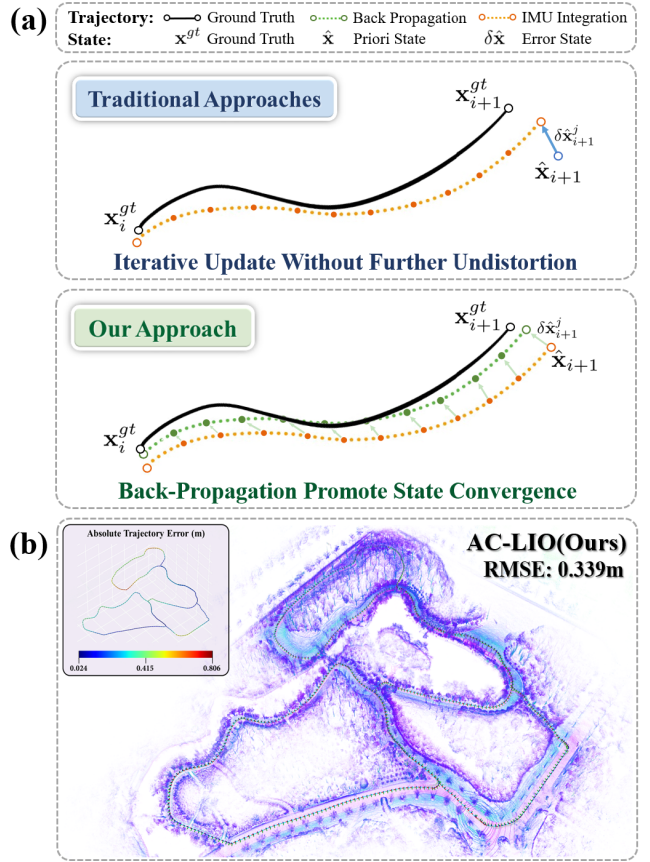


Fig. 1. (a) **A principal comparison of our AC-LIO with traditional approaches.** Conventional LIO typically considers an initial distortion compensation via IMU, yet the residual motion distortion may prevent the registration from further convergence. Our AC-LIO employs a selective intra-frame smoothing strategy to asymptotically backpropagate and compensate for residual distortion. (b) **Large scale localization and mapping result of BotanicGarden dataset.** We achieve better accuracy performance than other benchmark frameworks on its sequence Garden_1008 with VLP16 LiDAR.

LiDAR frames is often accompanied with the ego-motion of the vehicle, the LiDAR points with different timestamps actually lie in different coordinate systems.

As shown in Fig. 1, traditional methods [15]–[17] typically only consider using IMU integration for the initial compensation of motion distortion, without further optimization of the residual distortion in the state estimation. This residual motion distortion will compromise the consistency between the LiDAR frame with its corresponding geometric environment, and it grows with increasing motion non-linearity. Therefore, in conventional LIO systems, such residual error may suppress further convergence of pointcloud registration during the iterative update, ultimately impacting the odometry accuracy and causing severe drift.

Besides, we notice that few works directly apply the re-

liable and concise Rauch-Tung-Striebel (RTS) smoother for continuous optimization of motion distortion within discrete state LIO frameworks. While smoothing strategies have been widely adopted in continuous state estimation and several sliding window factor graph frameworks, they primarily focus on joint optimization across multiple states, which often leads to substantial computational consumption. However, since the LIO systems pursue a balance between real-time performance and accuracy, we seek a solution tailored for discrete state LIO frameworks that, without introducing additional estimates or state variables, leverage smoothing methods to achieve asymptotical compensation for residual motion distortion during iterative state estimation. Moreover, some redundant computation can be avoided as the state covariance chains are available from IMU prior propagation.

In this work, we propose AC-LIO, a novel discrete state LIO framework with selective intra-frame smoothing. Our AC-LIO introduces two key technical contributions. First, during iterative state estimation, we propose an *asymptotic distortion compensation* (Sec. III-C) method that backwards propagate the current update term based on the prior state chain, and asymptotically compensate for the residual distortion before next iteration. This approach could enhance the consistency between the current LiDAR frame and the represented geometric environment, and avoid the pointcloud registration from falling into local optimum due to the residual distortion, thereby promoting the accuracy of long-term and large-scene localization.

Second, due to the lack of correlation between initial error and motion distortion of current frame, we also propose the *convergence criteria* (Sec. III-D) based on the point-to-plane residuals to control the back propagation. We apply the criteria to assess the convergence of the pointcloud registration and ensure that the backpropagation and asymptotic compensation only happens under the condition of sufficient convergence in previous LiDAR frame, hence guaranteeing the robustness of LIO system. Compared to other strategies such as continuous-time estimation or frame segmentation, our method leverages this criteria to construct a feedback mechanism that promotes state convergence without additional estimation, achieving a balance between localization accuracy and computational efficiency (Sec. IV-E). It can be seamlessly embedded into the iterative Kalman Filter framework, offering great flexibility and scalability.

In summary, our main contributions are as follows:

- We propose a *novel* framework AC-LIO with *asymptotic distortion compensation* to further suppress residual distortion during iterative update, promoting system accuracy in long-term and large-scale scenarios.
- We introduce the *convergence criteria* based on point-to-plane residuals to evaluate the convergence and guide backpropagation. Backpropagation is only performed upon sufficient convergence of previous registration, thus further enhancing the system robustness.
- Compared to other optimization strategies for motion distortion, our framework introduce *no extra estimates or states*, making the asymptotic compensation less computationally expensive but highly flexible.

- We conduct extensive experiments on AC-LIO in a series of real-world datasets with various scenarios. The results show that our method achieves higher accuracy compared to current state-of-the-art frameworks. We also release our code to support and contribute to the open-source community.

II. RELATED WORK

LiDAR-Only Odometry. Studies such as LOAM [18] and F-LOAM [19] has achieved significant performance with the assumption of constant velocity motion during the corresponding time of LiDAR frames. However, this assumption only works effectively when LiDAR frame interval is enough short and the motion is slow and smooth. In case of drastic velocity variation, constant velocity model cannot accurately characterize current motion state, leading to increased drift and even odometry divergence. CT-ICP [20] optimize the start and end states of LiDAR frame, and construct a continuous time trajectory by interpolation. But the real movement may not follow the interpolated trajectory, as well as the logical constraint across adjacent frames is hard to determine. I²EKF-LO [21] utilizes extra prediction iteration to estimate motion distortion, yet the update of process noise still depends on some hyperparameters. Traj-LO [22] leverages high frequency of LiDAR points and employs more linear segments within frame. This approach allows more accurate trajectory characterization and suppression of motion aberrations during high speed motion, but also introduces more computational cost.

Discrete State LiDAR-Inertial Odometry. For LiDAR-inertial odometry, the IMU observation can provide relatively reliable prior state information. FAST-LIO2 [23] employs the IMU state backpropagation to correct the distorted pointcloud, and then conducts state estimation through Error State Kalman Filter. LIO-SAM [24] utilizes the IMU pre-integration to de-skew pointcloud, and fuses multiple constraints including LiDAR, IMU, and GPS through the factor graph. In the subsequent LIO frameworks, SR-LIO [25] adopts a LiDAR frame reconstruction strategy, while AS-LIO [26] designs an adaptive sliding window guided by spatial overlap degree, both of which can boost the system update frequency and lower the impact of motion distortion. Semi-Elastic-LIO [27] replaces the interpolation model with IMU motion constraints on the basis of CT-ICP framework, thereby improving the stability of the inter-frame logical constraints. Although these methods can mitigate the impact of pointcloud distortion to some extent, there are still some limitations without considering the further optimization of residual motion distortion. Point-LIO [28] adopts a point-by-point update strategy to avoid the motion distortion issue and realize extremely high-frequency odometry. Compared to frame based registration, the point-by-point strategy is more likely to be affected by dynamic objects and degenerate in adverse scenarios.

Continuous State LiDAR-Inertial Odometry. To characterize trajectories more precisely in state estimation, many frameworks come up with new optimization solutions. CLINS [29] introduces the B-spline for continuous state estimation, while SLICT [30] employs continuous-time factors to represent

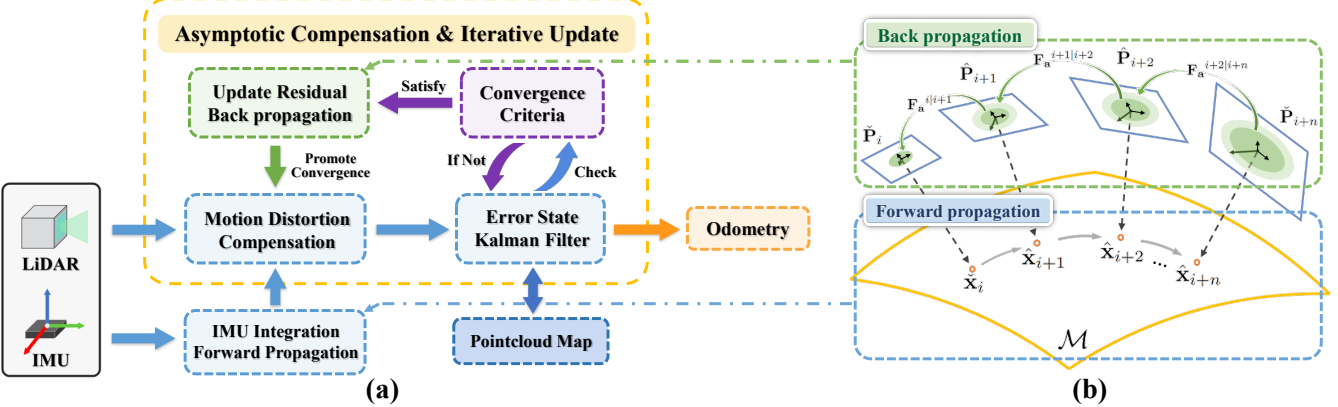


Fig. 2. (a) The system overview of our AC-LIO framework. During iterative ESKF, the back propagation and asymptotic compensation for pointcloud distortion are conducted based on the convergence criteria. (b) The on-manifold propagation. The blue shows the forward propagation of IMU integration. The green indicates the backward recursion of the update term according to the propagation matrix and noise relation of error state chains.

LiDAR constraints within a sliding window. However, the unconstrained trajectory would not always conform to predefined model due to time resolution limitations in high-speed, dynamic motion. Moreover, the continuous-time optimization strategy may introduce a higher computational cost. DLIO [31] uses analytical equations to model a continuous trajectory for precise motion correction, after coarse deskewing with IMU integration. Yet it remains limited by IMU's inherent accuracy and neglects further undistortion during registration process.

In contrast, our proposed AC-LIO framework utilizes the convergence criteria to guide the backpropagation and asymptotic compensation for residual motion distortion, further improving the accuracy over long-term and large-scale scenarios while ensuring the system robustness.

III. METHODOLOGY

A. System Overview

The system overview of our AC-LIO framework is shown in Fig. 2, and the important notations is shown in Table I. First, the IMU observations are fed into the forward propagation module to obtain prior trajectories. Then the LiDAR data utilize the prior state chain for initial compensation and then sent to the Error State Kalman Filter (ESKF) for state estimation [32], where the average point-to-plane residual (APR) is calculated after each update.

During the iteration, if the APR of previous LiDAR frame is lower than the convergence criteria and the current APR exceeds it, then the backpropagation of update residual will be executed. The LiDAR frame will be re-compensated to promote the convergence of registration after each backpropagation. Otherwise, if the conditions are not met, the backpropagation will be skipped and iteration continues. Once reaching the maximum of iterations, the system will merge the LiDAR frame under the posterior pose into pointcloud map and publish the current odometry.

B. ESKF State Estimation

For efficiency and accuracy concerns, the AC-LIO we proposed utilizes the ESKF framework for state estimation.

TABLE I
IMPORTANT NOTATIONS

Symbols	Definition
\boxplus/\boxminus	The boxplus and boxminus operators on manifold.
I, L, G	The IMU, LiDAR, and global coordinate frame.
\mathbf{x}^{gt}	The ground truth of state \mathbf{x} .
\mathbf{x}_i	The vector of state \mathbf{x} at timestamp i .
$\hat{\mathbf{x}}$	The priori estimation of state \mathbf{x} .
$\hat{\mathbf{x}}^j, \delta\hat{\mathbf{x}}^j$	The j -th update of state \mathbf{x} and error state $\delta\mathbf{x}$.
$\bar{\mathbf{x}}, \check{\mathbf{x}}$	The updated state \mathbf{x} with or without back propagation.
$\mathbf{F}_P^{i i+n}$	The propagation matrix from state i to $i+n$.
\mathbf{G}_i^{i+n}	The backward gain matrix of state i with respect to $i+n$.
\mathbf{z}, z	The vector and its scalar value of point-to-plane residual.
ϕ	The incident angle of single laser beam on the fitted plane.
σ_t	The expectation of average point-to-plane residual.

Based on the kinematic model and IMU measurement model, the state \mathbf{x} , input \mathbf{i} , and noise \mathbf{n} can be defined as follows:

$$\mathbf{x} \doteq [\mathbf{R}_I^G \quad \mathbf{p}_I^G \quad \mathbf{v}_I \quad \mathbf{b}_\omega \quad \mathbf{b}_a \quad \mathbf{g}^G]^T$$

$$\mathbf{i} \doteq [\omega_m \quad \mathbf{a}_m]^T, \quad \mathbf{n} \doteq [\mathbf{n}_\omega \quad \mathbf{n}_a \quad \mathbf{n}_{b\omega} \quad \mathbf{n}_{ba}]^T \quad (1)$$

Where \mathbf{R}_I^G , \mathbf{p}_I^G and \mathbf{v}_I^G are IMU's orientation, position and linear velocity in G , and \mathbf{g}^G is the local gravity. The \mathbf{n}_ω , \mathbf{n}_a are noises of angular velocity ω_m and linear acceleration \mathbf{a}_m , the \mathbf{b}_ω , \mathbf{b}_a are IMU bias with $\mathbf{n}_{b\omega}$ and \mathbf{n}_{ba} as their noises in Gaussian-Markov model. Since \mathbf{x} can be regarded as a high-dimensional manifold locally homeomorphic to Euclidean space \mathbb{R} . The operations \boxplus and \boxminus on manifold can be defined according to [33]. Note the error state as $\delta\mathbf{x}$, the recursion for $\delta\mathbf{x}$ and covariance \mathbf{P} can be expressed as follows:

$$\delta\mathbf{x}_i \doteq [\delta\theta \quad \delta\mathbf{p}_I^G \quad \delta\mathbf{v}_I \quad \delta\mathbf{b}_\omega \quad \delta\mathbf{b}_a \quad \delta\mathbf{g}^G]^T$$

$$\delta\hat{\mathbf{x}}_{i+1} = \mathbf{F}_P \delta\hat{\mathbf{x}}_i + \mathbf{F}_n \mathbf{n}_i \quad (2)$$

$$\hat{\mathbf{P}}_{i+1} = \mathbf{F}_P \hat{\mathbf{P}}_i \mathbf{F}_P^T + \mathbf{F}_n \mathbf{Q} \mathbf{F}_n^T$$

Assume the extrinsic \mathbf{T}_L^I between LiDAR and IMU is already known. For a point \mathbf{p} in LiDAR frame, its neighboring cluster can be searched by KNN in pointcloud map. If a plane S can be fitted to this cluster, then we will obtain its normal vector \mathbf{u} . Note one point of the cluster as \mathbf{q} and $(\cdot)_\wedge$ is

the upper triangular matrix of vector, then the point-to-plane residual \mathbf{z} and measurement matrix \mathbf{H} are as follows:

$$\begin{aligned} \mathbf{z} &= \mathbf{u}(\hat{\mathbf{p}}^G - \mathbf{q}^G)^T \\ \mathbf{H} &= [-\mathbf{u}\hat{\mathbf{R}}_I^G(\mathbf{T}_L^I \mathbf{p}^L)_{\wedge} \quad \mathbf{u} \quad \mathbf{0}_{3 \times 12}] \end{aligned} \quad (3)$$

Considering the nonlinear errors in the \mathbf{F}_p , \mathbf{F}_n and \mathbf{H} , the estimation may require iteration to promote convergence. Let \mathbf{A} denote the Jacobian of update component with respect to $\delta\mathbf{x}$, and according to [15], the update equation is:

$$\begin{aligned} \mathbf{K} &= \mathbf{P}\mathbf{H}^T(\mathbf{H}\mathbf{P}\mathbf{H}^T + \mathbf{R})^{-1} \\ \hat{\mathbf{x}}_{i+1}^{j+1} &= \hat{\mathbf{x}}_{i+1}^j \boxplus [-\mathbf{K}\mathbf{z} - (\mathbf{I} - \mathbf{K}\mathbf{H})(\mathbf{A}^j)^{-1}(\hat{\mathbf{x}}_{i+1}^j \boxminus \hat{\mathbf{x}}_{i+1}^j)] \end{aligned} \quad (4)$$

Once the update term is less than a preset threshold, the solution can be considered to converge.

$$\check{\mathbf{x}}_{i+1} \Leftarrow \hat{\mathbf{x}}_{i+1}^{j+1}, \check{\mathbf{P}}_{i+1} \Leftarrow (\mathbf{I} - \mathbf{K}\mathbf{H})\hat{\mathbf{P}}_{i+1} \quad (5)$$

With the iterative update of ESKF, our AC-LIO could further promote the convergence of the state estimation via the asymptotic distortion compensation and convergence criteria introduced in following sections.

C. Asymptotic Distortion Compensation

Compared to the noise of LiDAR observations, motion distortion may introduce bias in pointcloud registration, making it difficult to utilize the statistical properties of pointcloud to mitigate the adverse effects on state estimation.

During the on-manifold propagation of state \mathbf{x} , the noise of current error state $\delta\hat{\mathbf{x}}_{i+1}$ consists of the propagation of previous state $\delta\hat{\mathbf{x}}_i$ and the accumulated process noise. With reference to the Rauch-Tung-Striebel fixed interval smooth strategy [34], we can back propagate the update term $\delta\mathbf{x}$ based on the prior state chain. The contribution of previous state in current update term just corresponds to the proportion of propagation covariance $\mathbf{F}_p \hat{\mathbf{P}}_i \mathbf{F}_p^T$ within current covariance $\hat{\mathbf{P}}_{i+1}$. Then, the gain matrix \mathbf{G} and the backward recursion of $\delta\mathbf{x}$ can be denoted as follows:

$$\begin{aligned} \mathbf{G} &= \check{\mathbf{P}}_i \mathbf{F}_p^T \hat{\mathbf{P}}_{i+1}^{-1} \\ \delta\hat{\mathbf{x}}_i^j &= \mathbf{G} \cdot \delta\hat{\mathbf{x}}_{i+1}^j \end{aligned} \quad (6)$$

Furthermore, this sequential backpropagation method can be extend to any states within the LiDAR frame. It allows us to selectively update several anchor in the prior state chain, thus reducing the computational complexity of backpropagation and distortion compensation. As for any states \mathbf{x}_i and \mathbf{x}_{i+n} in the prior state chain, the propagation matrix and backward gain matrix can be noted as $\mathbf{F}_p^{i|i+n}$ and \mathbf{G}_i^{i+n} , then the backpropagation relationship should be:

$$\begin{aligned} \mathbf{F}_p^{i|i+n} &= \prod_{k=i}^{i+n-1} \mathbf{F}_p^{k|k+1} \\ \mathbf{G}_i^{i+n} &= \check{\mathbf{P}}_i (\mathbf{F}_p^{i|i+n})^T (\hat{\mathbf{P}}_{i+n})^{-1} \\ \check{\mathbf{x}}_i^j &= \check{\mathbf{x}}_i \boxplus (\mathbf{G}_i^{i+n} \cdot \delta\hat{\mathbf{x}}_{i+n}^j) \end{aligned} \quad (7)$$

After each backpropagation of the update term $\check{\mathbf{x}}_{i+n}^j$, where the j refers the current iteration times, the residual pointcloud distortion can continue to be compensated based on

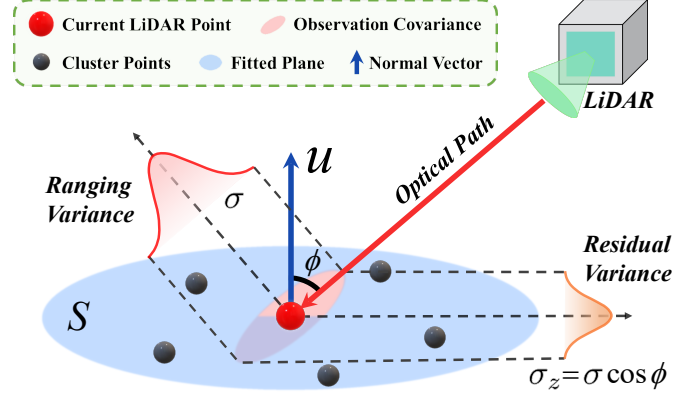


Fig. 3. The relationship between original ranging variance of LiDAR point and point-to-plane residual variance, where the residual z is a scalar.

the smoothed trajectory. For the point \mathbf{p}^L in LiDAR frame, and the state corresponding to its timestamp t after the j th backpropagation can be denoted as $\hat{\mathbf{x}}_t^j$, then the updated coordinates can be noted as:

$$\hat{\mathbf{p}}_j^G = \mathbf{T}(\hat{\mathbf{x}}_t^j) \mathbf{T}_L^I \mathbf{p}^L \quad (8)$$

Where $\mathbf{T}(\mathbf{x})$ represents the transformation matrix of state \mathbf{x} in frame G . As the iterative ESKF converges, the final solution of the backward propagation can be expressed as:

$$\check{\mathbf{x}}_i \Leftarrow \check{\mathbf{x}}_i^{j+1}, \check{\mathbf{P}}_i \Leftarrow \mathbf{G}_i^{i+n} \check{\mathbf{P}}_{i+n} (\mathbf{G}_i^{i+n})^T \quad (9)$$

In practice, if there is no need to reuse the previous state queue in next frame, the covariance update after backpropagation can be skipped for efficiency.

D. Convergence Criteria

Due to the lack of correlation between the previous error and the current motion distortion within a LiDAR frame, we find it necessary to introduce the convergence criteria to regulate the asymptotic distortion compensation. If the previous LiDAR frame has sufficiently converged, the current frame may start with a relatively small initial error, allowing the backpropagation to effectively compensate for motion distortion during iterative state estimation. However, if previous LiDAR frame has not converged well, then the initial error may degrade the system accuracy via the backpropagation. Therefore, a simple and efficient method is required to detect the convergence status of each LiDAR frame, in order to guide the asymptotic distortion compensation.

To exploit the statistical properties of pointcloud, during iterative state estimation, we select the mean value of the point-to-plane residual (abbreviated as APR above), as the criteria for evaluating the convergence of pointcloud registration. For simplification, assuming the pointcloud registration converges to the true pose and only considering the ranging accuracy of LiDAR, we can roughly model the expectation of the APR and provide a threshold reference for the convergence criteria.

Denote the incident angle of point \mathbf{p} to the fitted plane S as ϕ , it can be expressed as $\cos^{-1} \frac{|\mathbf{u} \cdot \hat{\mathbf{p}}^G|}{|\mathbf{u}| \cdot |\hat{\mathbf{p}}^G|}$ according to Eq. 3. Note that \mathbf{z} is the point-to-plane residual vector and

z is its scalar value. Assuming the ranging error of LiDAR point follows Gaussian distribution with zero mean and σ variance. When the laser beam is perpendicular to the fitted plane, the residual z_{\perp} follows chi-squared distribution and can be expressed as follows:

$$\begin{aligned} z_{\perp} &= |\mathbf{p}^G - \hat{\mathbf{p}}^G| \sim \mathcal{N}(0, \sigma) \\ \frac{z_{\perp}^2}{\sigma^2} &\sim \chi^2(1), \mathbb{E}(z_{\perp}) = \sigma \end{aligned} \quad (10)$$

As the surroundings vary during system's ego-motion, the distribution of normal vector \mathbf{u} to plane S also changes. The variation of the geometrical scene would be reflected in the distribution of the incident angle ϕ . From Fig. 3, the residual variance σ_z should be $\sigma \cos \phi$. Assuming the incident angle is uniformly distributed over the domain $[0, \pi/2]$, then the expected mean of point-to-plane residual can be expressed as:

$$\mathbb{E}(z) = \frac{2}{\pi} \int_0^{\frac{\pi}{2}} \mathbb{E}(z_{\perp}) \cos \phi \, d\phi = \frac{2}{\pi} \sigma \quad (11)$$

Therefore, assuming the pointcloud registration converges to the true pose, and only considering the LiDAR ranging error, the expectation of APR should be $2\sigma/\pi$. If the mean value of current point-to-plane residual is lower than this criteria, the last registration can be regarded as sufficiently converged.

Based on this threshold of convergence criteria, we can easily determine the convergence degree of pointcloud registration, and control the backpropagation and asymptotic distortion compensation. Noting that $\sigma_t = \mathbb{E}(z)$ and the selected threshold of convergence criteria as η , due to the factors such as dynamic objects and cumulative errors in pointcloud map, the threshold η can be appropriately extended to the interval of $[\sigma_t, 2\sigma_t]$ in practice. We collect a sequence of static-movement-static behavior with Livox AVIA, to evaluate the validity of our proposed convergence criteria. As shown in Fig. 8, the value of σ_t is very close to the APR during the static phases.

In detail, we perform two conditional judgments in iterative state estimation: First, evaluate the previous LiDAR frame, if its APR is less than the threshold η , it can be considered to be sufficiently converged and we will continue. Then, check the convergence of current registration, if the APR is still less than η , there is no need to backpropagate for small residual distortion; otherwise, we will perform the backpropagation and compensation during the iteration. On one hand, this approach can ensure the backpropagation and asymptotic compensation only performed as the previous LiDAR frame converged well, thus enhancing the odometry robustness in long-term and large-scale scenario. On the other hand, it can avoid lots of additional operations in unreliable or unnecessary conditions, to improve the system computational efficiency. The experiment results of our framework are shown in the next section.

IV. EXPERIMENT RESULTS

In this section, we qualitatively and quantitatively evaluate AC-LIO framework through a series of experiments with various public and self-collected datasets. To examine the performance of our approach in long-term and large-scale



Fig. 4. Our handheld sensor suite for self-collected dataset, including solid-state LiDAR Livox Avia with built-in BMI088 IMU, and three other cameras.

scenarios, we conduct extensive experiments on the odometry accuracy, the validity of convergence criteria, and the time efficiency of system.

A. Experiment Dataset

The datasets cover a wide range of structured environments (e.g., campus road and garage) and unstructured settings (e.g., botanical gardens), as well as different carriage modes (helmet, vehicle, handheld) to boost the challenge and completeness of assessment.

- WHU-Helmet [35]: Collected on compact helmet system with Livox LiDAR, the dataset contains complex large-scale scenes including wild, urban and tunnel, with challenges of drastic motion from wearer and repeated symmetrical geometric structures.
- BotanicGarden [36]: Mounted on all-terrain wheeled robot, this dataset consists of diverse natural scenes including riversides, narrow trails and bridges with both Livox Avia and VLP16 in sequence.
- Handheld datasets: We collected multiple datasets of different scenarios and motion conditions, covering indoor and outdoor scenes like library, campus road and UAV airfield with Livox Avia. The handheld data collection device is shown in Fig. 4.

B. Experiment Settings:

- We compared AC-LIO with current sota LIO frameworks that employ various methods to mitigate motion distortion, rather than LO frameworks without IMU integration. Some frameworks are designed for spinning LiDAR hence they are not included in comparison. Among the LIO frameworks, **FAST-LIO2** compensates for distortion via IMU prior trajectory before iterative estimation, **DLIO** applies a coarse-to-fine pointcloud deskewing approach, **SLICT** utilizes continuous-time state estimation to optimize the motion distortion, and **Point-LIO** is an extremely high frequency LIO with a point-by-point strategy to avoid motion distortion.

TABLE II
ODOMETRY ACCURACY EVALUATION - RMSE OF ATE & END TO END ERRORS(m)

Dataset	LiDAR Type	Sequence	Ours	FAST-LIO2	DLIO	SLICT	Point-LIO
WHU ¹ Helmet	Livox	Residence_5.2 (452.9m)	0.415	0.505	4.660	1.550	×
		Parking_3.2 (628.9m)	0.582	0.618	7.725	0.602	×
	AVIA	Subway_3.3 (827.0m)	1.670	3.752	3.688	<u>1.967</u>	×
		Mall_6.3 (1006.5m)	<u>0.216</u>	0.208	3.238	0.274	15.409
Botanic ¹ Garden	Livox	Garden_1005 (566.8m)	<u>0.773</u>	1.053	0.640	7.931	0.917
		Garden_1006 (686.2m)	1.796	<u>2.075</u>	3.017	6.527	2.471
		Garden_1008 (855.9m)	1.152	<u>1.577</u>	14.829	4.445	1.590
	VLP16	Garden_1005 (566.8m)	0.175	0.244	0.565	37.425	0.750
		Garden_1006 (686.2m)	0.377	<u>0.388</u>	0.393	×	0.445
		Garden_1008 (855.9m)	0.339	<u>0.363</u>	0.694	×	0.457
Handheld ²	Livox	Indoor_1 (~100m)	0.893	<u>1.133</u>	×	1.960	5.401
		Indoor_2 (~100m)	0.227	<u>0.204</u>	3.354	0.249	0.164
		Indoor_3 (~100m)	1.596	3.001	×	<u>2.476</u>	6.844
	AVIA	Outdoor_1 (~300m)	0.138	1.901	<u>0.486</u>	1.835	0.728
		Outdoor_2 (~400m)	0.984	2.194	7.879	1.803	<u>1.261</u>
		Outdoor_3 (~500m)	<u>2.666</u>	4.702	1.445	4.127	4.607
Average(RMSE)			0.750	<u>1.078</u>	3.945	7.590	3.148

¹ means the dataset is evaluated by RMSE of ATE, and ² means it is evaluated by End to End errors.

× denotes the system severely diverged midway, and denotes the second best result compared to bolded result.

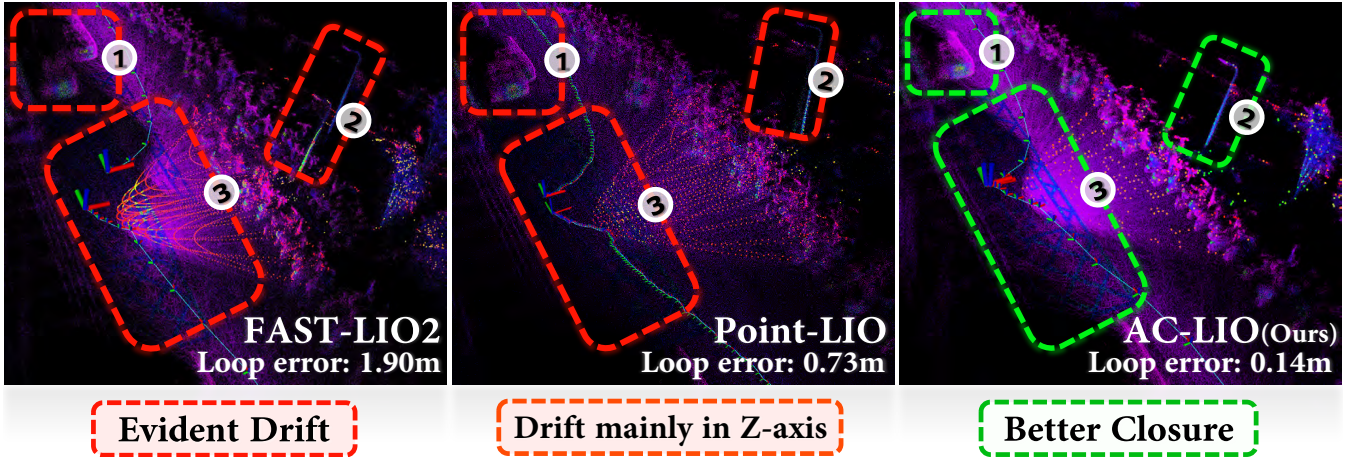


Fig. 5. Accuracy evaluation in campus road scene. The figure shows the result of sequence Outdoor_1. Within the dashed box are, in order, the car, the streetlight, and the pattern on the ground. We keep running after initialization to enhance the motion intensity and complete a closed loop about 300m. The closure trajectory and the map consistency suggest that our AC-LIO achieves better performance.

- All algorithms are implemented in C++ and employed on an i9 CPU computer with the ROS in Ubuntu. These methods only utilize CPU for computation without the assistance of GPU parallel computing. As our AC-LIO is implemented on the basis of FAST-LIO2, we control the same parameters especially with FAST-LIO2 (e.g., `imu_noise`, `voxel_size`, `max_iteration`, `point_filter_num`) for fair comparison. And we make every effort to fine-tune the parameters of other methods to achieve their best performance.
- Since our AC-LIO computes the convergence criteria to guide the asymptotic distortion compensation during iterative update, we fix the iteration times for every epoch (i.e., single LiDAR frame). In contrast, FAST-LIO2 jumps out the iteration as the update gradient belows a threshold, which may lead to an accuracy difference with our AC-LIO. Therefore, we conducted ablation studies specifically (Sec. IV-D) to validate the performance of

selective intra-frame smoothing.

C. Odometry Accuracy Evaluation

The odometry accuracy evaluation aims to demonstrate the overall accuracy performance of selected LIO frameworks and our AC-LIO. In the evaluation of WHU-Helmet, the sequences *Residence_5.2* and *Subway_3.3* introduce aggressive motion combined with locally degraded scenarios, while *Parking_3.2* and *Mall_6.3* suffer from extensive occlusion by pedestrians. These factors impose higher demands on the robustness of the LIO system. For the BotanicGarden datasets, we test both the solid-state (Livox AVIA) and the spinning (VLP16) LiDAR. Since the sensors are mounted on a wheeled robotic platform, the overall motion is smooth and suitable for evaluating long-duration drift under regular motion conditions. However, the abundance of unstructured scenes in the garden (e.g., thick woods, bushes) poses challenges for constructing residual constraints. In our self-collected datasets, we handhold the sensor

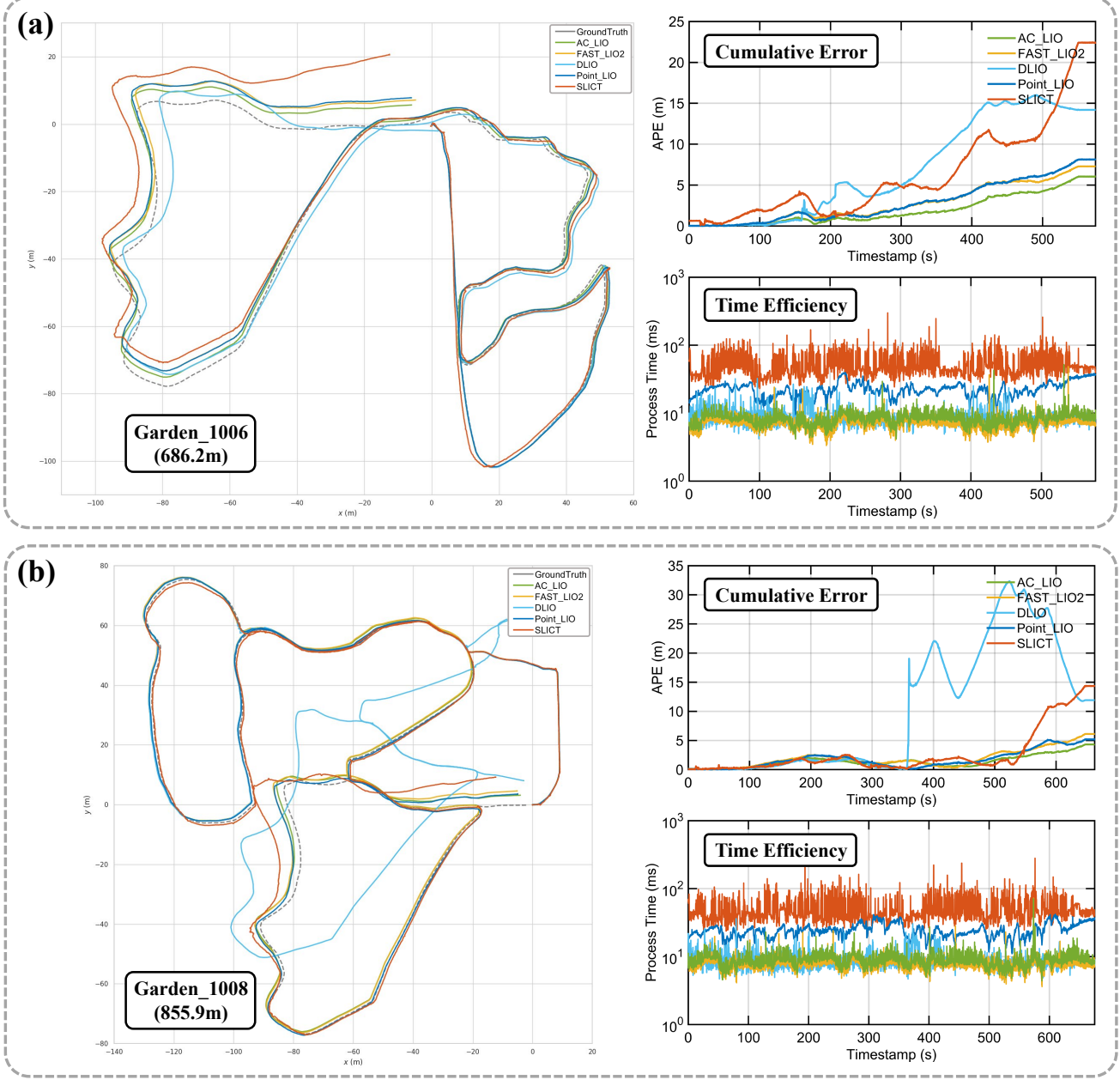


Fig. 6. Accuracy evaluation in Botanic Garden dataset. The figure shows the result of sequence (a) **Garden_1006** and (b) **Garden_1008**. For each sequence, the left part presents the trajectory comparison, with the top 10% states aligned to the ground truth, and the right part displays the cumulative error curve of APE (m) along with the corresponding real-time process efficiency. The results suggest that our AC-LIO achieves lower cumulative error while maintaining relatively good time efficiency (Sec. IV-E). The average runtime of our method is only slightly higher than the FAST-LIO2 framework.

suite and completed multiple closed-loop paths in different scenarios. In *Indoor_1* UAV airfield and *Indoor_3* library scenarios, we conduct intense turning in narrow environment. For the *Outdoor* sequences, we handheld the device and attempt different motion conditions including running and sharp turns in campus road scenes.

Concrete experiment results are demonstrated in Table II, Fig. 5 and Fig. 6. Our approach further optimizes the residual motion distortion via selective intra-frame smoothing strategy, thus improving the accuracy while ensuring the robustness of the system under challenging scenarios. The results indicate that our AC-LIO method generally outperforms other benchmark frameworks in terms of accuracy during long-term,

large-scale scenes, with the average RMSE among sequences decreased by 30.4% compared to the second best, and exhibits high robustness under challenging scenarios.

D. Convergence Criteria Evaluation

To evaluate the rationality and validity of the proposed convergence criteria, we conduct two type of experiments. **Rationality:** Since the modeling of convergence criteria involves certain simplification and assumption, we examine the rationality through comparing the actual APR values with the theoretical value of σ_t , as the APR during static phase can be regarded as a reference of σ_t under ideal conditions. We collect a static-movement-static sequence with Livox AVIA.

TABLE III
CONVERGENCE CRITERIA VALIDITY EVALUATION - RMSE OF ATE (m)

Sequence	LiDAR	FAST-LIO2	$0\sigma_t$	$0.5\sigma_t$	$1\sigma_t$	$1.5\sigma_t$	$2\sigma_t$	$2.5\sigma_t$	$3\sigma_t$
Garden_1005 (566.8m)	AVIA	1.053	1.063	1.063	1.004	0.943	0.743	<u>0.907</u>	1.120
	VLP16	0.244	0.244	0.241	0.226	0.175	<u>0.193</u>	0.208	0.233

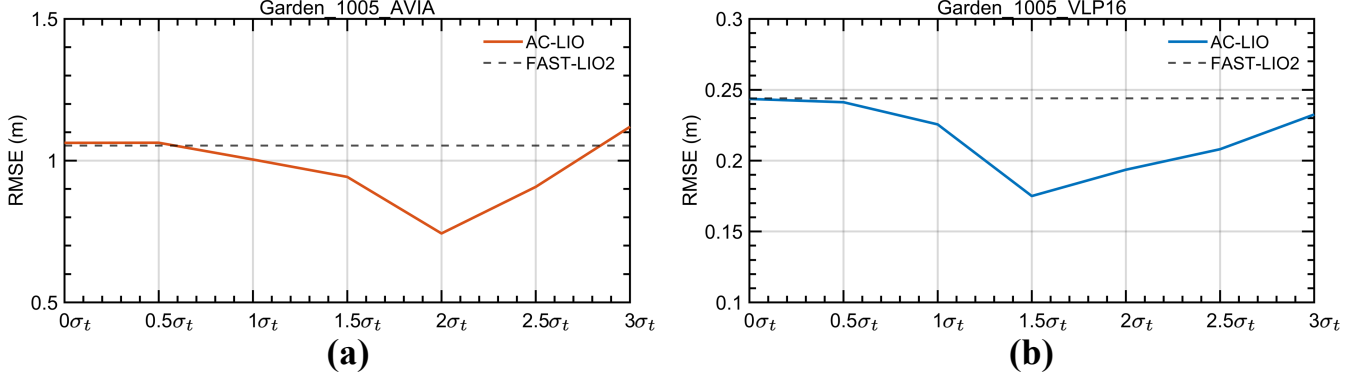


Fig. 7. **Validity evaluation of convergence criteria.** These two figures present the ablation experiments on convergence criteria using Garden_1005 sequence: (a) for Livox AVIA and (b) for VLP16, showing the generalization between different LiDAR sensors. The gray dashed line refers the accuracy of FAST-LIO2. As threshold η increases from zero, the accuracy improves because more sufficiently converged states are allowed to perform backpropagation. However, as η continues to increase, states with larger initial errors are also allowed to backpropagate, which gradually degrades the overall accuracy.

As shown in Fig. 8, the actual APR values during the static phases are very close to σ_t , indicating good consistency between theoretical derivation of σ_t and actual APR results. Furthermore, the APR increases and becomes more volatile during the movement phase. Too large an APR reflects a higher risk of insufficient convergence. We introduce the convergence criteria to prevent the asymptotic distortion compensation from starting with too high an initial error.

Validity: We examine the accuracy of AC-LIO at different η threshold levels for both AVIA and VLP16, and compare with the benchmark of FAST-LIO2. While keeping other parameters the same, we only adjust the threshold of convergence criteria. The experimental results are shown in Table III and Fig. 7.

- $\eta \in [0, 0.5\sigma_t]$: No or rare backpropagation and asymptotic compensation is performed under this condition, reflecting the basic odometry accuracy.
- $\eta \in [\sigma_t, 2\sigma_t]$: Recommended interval in consideration of other error factors, assuring the backpropagation and asymptotic compensation will be performed with sufficient convergence in previous frame.
- $\eta \in [2.5\sigma_t, 3\sigma_t]$: Too high a threshold may lead to the backpropagation in case of large initial errors, potentially degrade the overall system accuracy and robustness.

The results show that, in most cases, selecting the threshold η within the range of $[\sigma_t, 2\sigma_t]$ can achieve higher accuracy. As the threshold increases from zero, the odometry accuracy initially improves because more sufficiently converged states are allowed to perform backpropagation and asymptotic compensation. However, as the threshold increases further, states with larger initial errors are also allowed to backpropagate, which reduces the effectiveness of the asymptotic compensation and gradually impacts odometry accuracy.

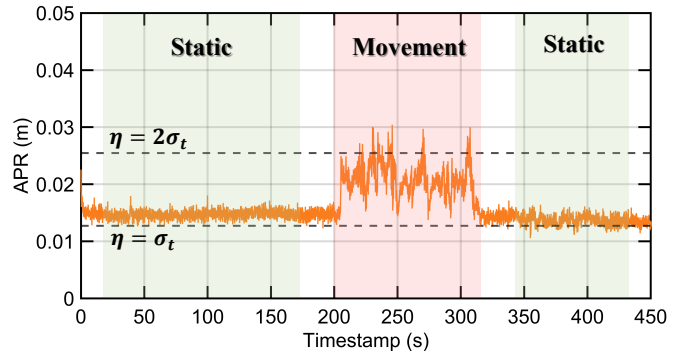


Fig. 8. **Rationality evaluation of convergence criteria.** The orange curve refers the average point-to-plane residual (APR) during a static-movement-static sequence in an indoor scenario. The APR values under static phases are very closed to the theoretical value of σ_t , indicating good consistency between theoretical derivation and actual APR results.

E. Time Efficiency Evaluation

We calculate the runtime of each algorithm during iteration, with the results shown in Table IV and Fig. 9. And the specific runtime curves can be found in Fig. 7. In terms of average processing time, the time efficiency of our AC-LIO framework ranks second place among the tested frameworks, just following the FAST-LIO2 framework and comparable to the lightweight DLIO framework. The maximum time for iteration also satisfies realtime requirement (below 100ms for 10Hz LiDAR input). Due to the convergence criteria strategy, our method can avoid incurring extra optimization costs in unreliable or unnecessary conditions, thus achieving the balance between system convergence and high time efficiency.

V. CONCLUSION

In this paper, we proposed AC-LIO, a novel discrete state LIO framework with selective intra-frame smoothing. We

TABLE IV
TIME CONSUMPTION EVALUATION (ms)

	Ours	FAST-LIO2	DLIO	SLICT	Point-LIO
Min	4.12	2.89	3.95	22.61	7.83
Max	70.69	66.38	37.22	460.24	50.84
Mean	<u>8.55</u>	7.18	8.57	48.62	24.48
Median	8.316	6.971	8.24	42.91	23.61

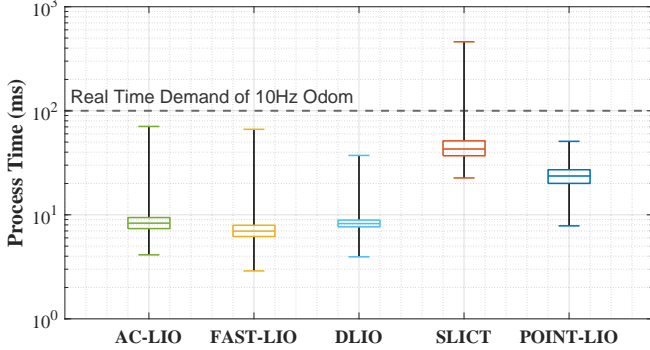


Fig. 9. **Time efficiency evaluation.** The cross line inside box denotes the median process time. Our AC-LIO achieves the second highest efficiency, only behind the FAST-LIO2 and comparable to the lightweight DLIO. The maximum runtime also meets the real-time requirements.

reconsider the factors that may introduce errors in long-duration, large-scale scenarios, aiming to further enhance the convergence of LIO system. The approach of guiding asymptotic compensation based on convergence criteria is designed to further suppress the motion distortion within LiDAR frame, improving the odometry accuracy while ensuring system robustness. Extensive experiments indicate that our framework achieves an average RMSE reduction of approximately 30.4% over the second best method, demonstrating higher accuracy in long-term, large-scale localization and mapping. In terms of time efficiency, our framework ranks second place among the evaluated frameworks, just following the FAST-LIO2 and comparable to the lightweight DLIO, achieving a balance between accuracy and real-time performance.

REFERENCES

- [1] H. Taheri and Z. C. Xia, "Slam; definition and evolution," *Engineering Applications of Artificial Intelligence*, vol. 97, p. 104032, 2021.
- [2] C. Cadena, L. Carlone, H. Carrillo, Y. Latif, D. Scaramuzza, J. Neira, I. Reid, and J. J. Leonard, "Past, present, and future of simultaneous localization and mapping: Toward the robust-perception age," *IEEE Transactions on robotics*, vol. 32, no. 6, pp. 1309–1332, 2016.
- [3] Y. Chen, S. Huang, and R. Fitch, "Active slam for mobile robots with area coverage and obstacle avoidance," *IEEE/ASME Transactions on Mechatronics*, vol. 25, no. 3, pp. 1182–1192, 2020.
- [4] H. Wang, C. Wang, and L. Xie, "Intensity-slam: Intensity assisted localization and mapping for large scale environment," *IEEE Robotics and Automation Letters*, vol. 6, no. 2, pp. 1715–1721, 2021.
- [5] R. Duan, D. P. Paudel, C. Fu, and P. Lu, "Stereo orientation prior for uav robust and accurate visual odometry," *IEEE/ASME Transactions on Mechatronics*, vol. 27, no. 5, pp. 3440–3450, 2022.
- [6] X. Wang, X. Li, H. Yu, H. Chang, Y. Zhou, and S. Li, "Givl-slam: A robust and high-precision slam system by tightly coupled gnss rtk, inertial, vision, and lidar," *IEEE/ASME Transactions on Mechatronics*, 2024.
- [7] J. Lv, X. Lang, J. Xu, M. Wang, Y. Liu, and X. Zuo, "Continuous-time fixed-lag smoothing for lidar-inertial-camera slam," *IEEE/ASME Transactions on Mechatronics*, vol. 28, no. 4, pp. 2259–2270, 2023.
- [8] L. Jin, H. Zhang, and C. Ye, "Camera intrinsic parameters estimation by visual-inertial odometry for a mobile phone with application to assisted navigation," *IEEE/ASME Transactions on Mechatronics*, vol. 25, no. 4, pp. 1803–1811, 2020.
- [9] B. Han, Y. Lin, Y. Dong, H. Wang, T. Zhang, and C. Liang, "Camera attributes control for visual odometry with motion blur awareness," *IEEE/ASME Transactions on mechatronics*, vol. 28, no. 4, pp. 2225–2235, 2023.
- [10] Z. Song, X. Zhang, T. Li, S. Zhang, Y. Wang, and J. Yuan, "Ir-vio: Illumination-robust visual-inertial odometry based on adaptive weighting algorithm with two-layer confidence maximization," *IEEE/ASME Transactions on Mechatronics*, vol. 28, no. 4, pp. 1920–1929, 2023.
- [11] D. Lee, M. Jung, W. Yang, and A. Kim, "Lidar odometry survey: recent advancements and remaining challenges," *Intelligent Service Robotics*, vol. 17, no. 2, pp. 95–118, 2024.
- [12] K. Li, M. Li, and U. D. Hanebeck, "Towards high-performance solid-state-lidar-inertial odometry and mapping," *IEEE Robotics and Automation Letters*, vol. 6, no. 3, pp. 5167–5174, 2021.
- [13] Z. Liao, X. Zhang, T. Zhang, Z. Li, Z. Zheng, Z. Wen, and Y. Li, "A real-time degeneracy sensing and compensation method for enhanced lidar slam," *IEEE Transactions on Intelligent Transportation Systems*, 2025.
- [14] M. McDermott and J. Rife, "Correcting motion distortion for lidar scan-to-map registration," *IEEE Robotics and Automation Letters*, vol. 9, no. 2, pp. 1516–1523, 2023.
- [15] W. Xu and F. Zhang, "Fast-lio: A fast, robust lidar-inertial odometry package by tightly-coupled iterated kalman filter," *IEEE Robotics and Automation Letters*, vol. 6, no. 2, pp. 3317–3324, 2021.
- [16] J. Xu, Y. Ma, Y. Li, X. Zhang, J. Zhou, S. Yuan, and L. Xie, "Dynamic initialization for lidar-inertial slam," *IEEE/ASME Transactions on Mechatronics*, 2025.
- [17] Y. Wu and J. Zhao, "A robust and precise lidar-inertial-gps odometry and mapping method for large-scale environment," *IEEE/ASME Transactions on Mechatronics*, vol. 27, no. 6, pp. 5027–5036, 2022.
- [18] J. Zhang, S. Singh *et al.*, "Loam: Lidar odometry and mapping in real-time," in *Robotics: Science and systems*, vol. 2, no. 9. Berkeley, CA, 2014, pp. 1–9.
- [19] H. Wang, C. Wang, C.-L. Chen, and L. Xie, "F-loam: Fast lidar odometry and mapping," in *2021 IEEE/RSJ International Conference on Intelligent Robots and Systems (IROS)*. IEEE, 2021, pp. 4390–4396.
- [20] P. Dellenbach, J.-E. Deschaud, B. Jacquet, and F. Goulette, "Ct-icp: Real-time elastic lidar odometry with loop closure," in *2022 International Conference on Robotics and Automation (ICRA)*. IEEE, 2022, pp. 5580–5586.
- [21] W. Yu, J. Xu, C. Zhao, L. Zhao, T.-M. Nguyen, S. Yuan, M. Bai, and L. Xie, "I2ekf-lo: A dual-iteration extended kalman filter based lidar odometry," *arXiv preprint arXiv:2407.02190*, 2024.
- [22] X. Zheng and J. Zhu, "Traj-lo: In defense of lidar-only odometry using an effective continuous-time trajectory," *IEEE Robotics and Automation Letters*, vol. 9, no. 2, pp. 1961–1968, 2024.
- [23] W. Xu, Y. Cai, D. He, J. Lin, and F. Zhang, "Fast-lio2: Fast direct lidar-inertial odometry," *IEEE Transactions on Robotics*, vol. 38, no. 4, pp. 2053–2073, 2022.
- [24] T. Shan, B. Englot, D. Meyers, W. Wang, C. Ratti, and D. Rus, "Lio-sam: Tightly-coupled lidar inertial odometry via smoothing and mapping," in *2020 IEEE/RSJ international conference on intelligent robots and systems (IROS)*. IEEE, 2020, pp. 5135–5142.
- [25] Z. Yuan, F. Lang, T. Xu, and X. Yang, "Sr-lo: Lidar-inertial odometry with sweep reconstruction," in *2024 IEEE/RSJ International Conference on Intelligent Robots and Systems (IROS)*. IEEE, 2024, pp. 7862–7869.
- [26] T. Zhang, X. Zhang, Z. Liao, X. Xia, and Y. Li, "As-lo: Spatial overlap guided adaptive sliding window lidar-inertial odometry for aggressive fov variation," in *2024 IEEE/RSJ International Conference on Intelligent Robots and Systems (IROS)*. IEEE, 2024, pp. 10829–10836.
- [27] Z. Yuan, F. Lang, T. Xu, R. Ming, C. Zhao, and X. Yang, "Semi-elastic lidar-inertial odometry," *arXiv preprint arXiv:2307.07792*, 2023.
- [28] D. He, W. Xu, N. Chen, F. Kong, C. Yuan, and F. Zhang, "Point-lo: Robust high-bandwidth light detection and ranging inertial odometry," *Advanced Intelligent Systems*, vol. 5, no. 7, p. 2200459, 2023.
- [29] J. Lv, K. Hu, J. Xu, Y. Liu, X. Ma, and X. Zuo, "Clins: Continuous-time trajectory estimation for lidar-inertial system," in *2021 IEEE/RSJ International Conference on Intelligent Robots and Systems (IROS)*. IEEE, 2021, pp. 6657–6663.
- [30] T.-M. Nguyen, D. Duberg, P. Jensfelt, S. Yuan, and L. Xie, "Slicht: Multi-input multi-scale surfel-based lidar-inertial continuous-time odometry and mapping," *IEEE Robotics and Automation Letters*, vol. 8, no. 4, pp. 2102–2109, 2023.

- [31] K. Chen, R. Nemiroff, and B. T. Lopez, “Direct lidar-inertial odometry: Lightweight lio with continuous-time motion correction,” in *2023 IEEE international conference on robotics and automation (ICRA)*. IEEE, 2023, pp. 3983–3989.
- [32] J. Sola, “Quaternion kinematics for the error-state kf,” *Laboratoire d’Analyse et d’Architecture des Systèmes-Centre national de la recherche scientifique (LAAS-CNRS), Toulouse, France, Tech. Rep*, p. 35, 2012.
- [33] C. Hertzberg, R. Wagner, U. Frese, and L. Schröder, “Integrating generic sensor fusion algorithms with sound state representations through encapsulation of manifolds,” *Information Fusion*, vol. 14, no. 1, pp. 57–77, 2013.
- [34] A. Gelb, *Applied Optimal Estimation*. MIT Press, 1974.
- [35] J. Li, W. Wu, B. Yang, X. Zou, Y. Yang, X. Zhao, and Z. Dong, “Whu-helmet: a helmet-based multisensor slam dataset for the evaluation of real-time 3-d mapping in large-scale gnss-denied environments,” *IEEE Transactions on Geoscience and Remote Sensing*, vol. 61, pp. 1–16, 2023.
- [36] Y. Liu, Y. Fu, M. Qin, Y. Xu, B. Xu, F. Chen, B. Goossens, P. Z. Sun, H. Yu, C. Liu *et al.*, “Botanicgarden: A high-quality dataset for robot navigation in unstructured natural environments,” *IEEE Robotics and Automation Letters*, 2024.